

CERN

A 3
BIBLIOGRAPHY 26 AUG 1985

TRI-PP-85-14
Mar 1985

TRI-PP 85-14

CM-P00067378

- 2 -

Search for μ -e conversion in Ti

D.A. Bryman, E.T.H. Clifford, M.J. Leitch*, I. Navon,

T. Numao ** and P. Schlatter

TRIUMF and University of Victoria, Vancouver, B.C., Canada V6T 2A3

M.S. Dixit, C.K. Hargrove, and H. Mes

National Research Council of Canada, Ottawa, Ontario, Canada K1A 0R6

R.A. Burnham, M. Hasinoff, and J.-M. Poutissou

TRIUMF and University of British Columbia, Vancouver, B.C., Canada V6T 2A3

J.A. Macdonald and J. Spuller

TRIUMF, Vancouver, British Columbia, Canada V6T 2A3

G. Azuelos**, P. Depommier, J.-P. Martin and R. Poutissou

Université de Montréal, Montréal, Québec, Canada H3C 3J7

etc. 2-5 In some models, mass limits in the multi-TeV range have been

M. Blecher and K. Gott

Virginia Polytechnic Institute and State University, †
Blacksburg, Virginia 24061

A.L. Carter

Carleton University, Ottawa, Ontario, Canada K1S 5B6

H.L. Anderson

LASL, Los Alamos, New Mexico 87545

S.C. Wright

University of Chicago, Chicago, Illinois 60637

$$\mu^- + Z \rightarrow e^- + Z \quad (1)$$

has been discussed as a potentially favorable process with which to search for lepton flavor violation.¹ Many attempts to incorporate multiple generations (flavors) into the standard model of weak interactions predict branching ratios for lepton flavor changing processes, such as μ -e conversion (1), $\mu + e\gamma$ and $\mu + 3e$, at the level of $< 10^{-9}$ relative to ordinary flavor conserving processes, depending on the masses and couplings of hypothetical neutral leptons, gauge bosons, etc.²⁻⁵ In some models, mass limits in the multi-TeV range have been obtained from the experimental upper limits for these reactions. The signature of coherent μ -e conversion (1) in which the nucleus remains in the ground state is a single peak at the electron energy $E_e \sim m_\mu c^2/B$, where m_μ and B are the muon mass (105.7 MeV/c 2) and the binding energy of the muonic atom, respectively. The incoherent reaction leading to excited nuclear states is suppressed because of the Pauli blocking effect. Previous searches for coherent μ -e conversion using copper and sulphur targets have led to limits (90% C.L.)

$$\frac{\Gamma(\mu^-Cu \rightarrow e^-Cu)}{\Gamma(\mu^-Cu \rightarrow \text{capture})} < 1.6 \times 10^{-8} \quad (\text{Ref. 6})$$

and

$$\frac{\Gamma(\mu^-S \rightarrow e^-S)}{\Gamma(\mu^-S \rightarrow \text{capture})} < 7 \times 10^{-11} \quad (\text{Ref. 7}).$$

In this letter, a new upper limit for μ -e conversion in titanium ($E_e \sim 10^4$ MeV) is reported.

The detection system is based on a hexagonal time projection chamber (TPC) shown in Fig. 1. The titanium target is mounted on the TPC axis surrounded by inner trigger counters consisting of six plastic scintillators and a cylindrical wire chamber. The outer trigger counters

Present address: *LASL, Los Alamos, New Mexico 87545

**TRIUMF, 4004 Wesbrook Mall, Vancouver, B.C., Canada

†Supported in part by the National Science Foundation

consist of six planar wire chambers each sandwiched between two plastic scintillators. On the top and sides of the magnet are two layers of drift chambers for detecting cosmic ray initiated events.

The TRIUMF TPC8,⁹ is a large volume atmospheric-pressure drift chamber situated in axially parallel magnetic and electric fields.

Table I gives some of the TPC characteristics. Ionization electrons from a charged particle track drift to the endcaps of the chamber, where they are detected by a proportional wire system which gives independent x, y and z coordinates. The position of each anode wire determines the y coordinate. The distribution of induced charges on the cathode, segmented into pads along the direction of the wire, is used to find the coordinate, x, along the anode wire. Using the drift velocity in the gas, the drift time of the track segment to each wire gives the axial coordinate, z.

The apparatus was set up at the end of the M9 channel at TRIUMF. A 73 MeV/c μ^- beam was stopped at a typical rate of 5×10^5 s⁻¹ in a 20 cm long shredded natural Ti target with a density of 0.1 g cm⁻³. The raw μ^- beam contained a similar flux of pions and an order of magnitude more electrons. Because the π^- contamination in the beam can cause backgrounds in the E_e=100 MeV region through radiative capture reactions, an RF particle separator¹⁰ in the beam channel was used to reduce the pion and electron contaminations to $\pi/\mu \approx 10^{-4}$ and $e/\mu \approx 10^{-2}$ at the stopping target.

A valid stop signal opened a 600 ns wide time gate during which an electron trigger, defined as a coincidence of both inner counter layers and at least two of the three outer layers, could be accepted. The trigger signal gated grids⁹ on the appropriate TPC sectors, allowing

ionization tracks to drift onto the end caps. Signals from > 6 wires of the TPC were required in the event trigger. The magnetic field of 9 kG prevented most $\mu \rightarrow e\bar{v}v$ decay electrons from reaching the outer trigger counters. The typical event rate of 3 s⁻¹ was due mostly to protons from μ^- capture reactions and low energy electrons in coincidence with associated bremsstrahlung photons which fired the outer trigger detectors.

The efficiency and resolution of the detector system were monitored at regular intervals with mono-energetic positrons (70 MeV/c) from the decay $\pi^+ \rightarrow e^+\nu$. For these tests, the magnetic field was lowered to 6 kG to reproduce the curvature of ~100 MeV/c μ^+ e events at 9 kG. The pion beam rate was adjusted to keep counting rates in the TPC comparable to those of the μ^- data runs.

The data analysis was done in several steps. First, the initial 2×10^7 events on tape were searched for tracks having > 6 valid (X,Y,Z) points in the TPC and these were fitted to a helix by minimizing χ^2 . The momentum, energy loss, origin of the track and other quantities were obtained from the fit and loose cuts were applied. The surviving data (approximately 10^6 events) were then subjected to more stringent cuts. The data included background events due to cosmic rays and beam pions, which were tagged by the cosmic ray veto counters and beam scintillators, respectively. Since such tracks had quite different origin distributions from muon initiated events, a target position cut was effective in reducing these backgrounds. A χ^2 cut was used to remove events for which the track fit was unreliable.

The remaining μ^+ e candidates and $\mu^+\nu\bar{e}v$ events above momentum P=80 MeV/c, approximately 1000 events, were plotted for visual inspection. About 95% of the events passed this inspection. A momentum

spectrum of those electron events with $P > 87$ MeV/c is shown by the solid line histogram in Fig. 2. No candidate events were observed in the 97 to 105.5 MeV/c region. The expected number of events in this region due to cosmic rays and beam pions was estimated to be less than one.

Since the $\pi \rightarrow e\nu$ data were taken under conditions similar to the $\mu\bar{e}$ runs, the acceptances measured in $\pi\bar{e}\nu$ runs included the efficiency losses due to most cuts. Corrections for the other cuts, such as the target position cut, were applied separately (because of the different stopping distributions of the pion and muon beams). A typical acceptance determined from the $\pi\bar{e}\nu$ runs was ~12%. Average correction factors applied to the acceptance due to the various cuts are listed in Table II.

Correction for the momentum window difference between the 67 MeV/c $\pi\bar{e}\nu$ peak and the expected 101 MeV/c $\mu\bar{e}$ peak (including a 3 MeV/c loss) was determined by Monte Carlo calculation. The momentum resolution for the $\pi\bar{e}\nu$ peak, 6 MeV/c (FWHM), was reproduced by the Monte Carlo calculation using position resolutions obtained from high energy cosmic ray events. The calculation included all energy losses in the target, in the material inside the TPC and in the TPC gas, and the effect of $\vec{E} \times \vec{B}$ forces⁸ on the track segments near the anode wires. (The latter effect results in a degradation of the resolution for positively charged particles compared to negatively charged ones.) The result of a Monte Carlo calculation corresponding to a branching ratio of 10^{-10} is shown by the dashed line in Fig. 2. The expected resolution of the $\mu\bar{e}$ conversion peak is 5 MeV/c (FWHM). The momentum window of 97~105.5 MeV/c for the observed spectrum would include 80% of all $\mu \rightarrow e$ conversion events.

The efficiency loss due to the π background cut was deduced from the $\mu\bar{e}$ runs by comparing the numbers of pion and non-pion associated events in the momentum region 60~70 MeV/c, where $\mu\bar{e}\nu\bar{\nu}$ events are dominant. The multiplicative factor applied to the acceptance was 0.9. The

correction for the 50~600 ns software time window on the muon capture lifetime in Ti was 0.7, which also included the timing spectrum distortion due to extra muons in the target. The correction factor of 0.9 for the target position cut was estimated from runs taken at a lower magnetic field to accept more $\mu\bar{e}\nu\bar{\nu}$ decay events. The correction factor for the χ^2 cut and the visual inspection was estimated to be 0.9 from $\mu\bar{e}\nu\bar{\nu}$ events in the 80~83 MeV/c region.

The acceptance was calculated for each running period. The average net efficiency over all running periods was $\bar{\Omega} \sim 4\%$. The number of muon stops in the Ti target was corrected for inefficiencies of the veto counters. This correction was deduced from the decay curve of $\mu\bar{e}\nu\bar{\nu}$ events by fitting it with two decay components, $\tau_1=329.3$ ns for μ^- in titanium and $\tau_2=2026.3$ ns for μ^- in carbon.¹¹ A typical correction factor was 0.9.

Based on the absence of candidate events in 5×10^{12} stopped muons and assuming the Poisson distribution, the upper limit of the branching ratio for the reaction (1) is

$$R \equiv \frac{\Gamma(\mu^- + Ti + e^- + Ti)}{\Gamma(\mu^- + Ti + \text{capture})} < \frac{2.3}{0.853 \sum_i N_i \Omega_i}$$

$$R < 1.6 \times 10^{-11} \text{ (90\% C.L.)},$$

where N_i is the number of stopped muons in Ti , Ω_i is the efficiency for a specific run period, i , and 0.853 is the μ^- -capture ratio in Ti . The confidence level does not include an estimated uncertainty of 20% in the

efficiency. The solid line in Fig. 2 shows the result of Monte Carlo calculations for $\mu \rightarrow e\bar{v}v$ decay-in-orbit events corresponding to the present data. The spectrum was obtained from parametrization and interpolation of the calculations by Herzog and Alder¹² for Ar, Ca and Fe with V-A couplings. The parametrization is valid within 20% for the region above 60 MeV/c. Good agreement between the calculation and the data was obtained.

The contribution from radiative μ capture was less than 5% of $\mu \rightarrow e\bar{v}v$ events and was neglected.

A branching ratio for incoherent processes was estimated to be $(0.5 \pm 2.1) \times 10^{-10}$ for the momentum region above 87 MeV/c by taking the difference between the experimental and the Monte Carlo $\mu \rightarrow e\bar{v}v$ spectra. The statistical error and the systematic errors in the normalization and in the Monte Carlo calculation were added quadratically. The dependence of the acceptance on momentum was obtained by Monte Carlo calculations.

The cut-off momentum of 87 MeV/c corresponds to an excitation energy $E_X = 14$ MeV of the residual nucleus. The photon spectrum from the $^{40}\text{Ca}(\pi^-, \gamma) X$ reaction¹³ was used to estimate the expected electron spectrum shape in the incoherent process for the momentum region below 87 MeV/c, since, kinematically, the incoherent $\mu \rightarrow e$ process is similar to the radiative capture of pions (π^-, γ) at rest. The fraction of the events below $E_X = 14$ MeV in the efficiency-corrected (π^-, γ) spectrum gave a multiplicative correction factor of 6.2. This led to an upper limit of 1.9×10^{-9} (90% C.L.) for the ratio of incoherent $\mu \rightarrow e$ conversion to the normal capture process.

According to Shanker,¹⁴ for the vector current case the coherent $\mu \rightarrow e$ conversion branching ratio can be expressed phenomenologically as the sum of isoscalar (g^0) and isovector (g^1) terms, arising from different

couplings to up and down quarks. Using the present upper limit and the result of Ref. 7, the limit on g^1 is

$$|g^1| < 3.5 \times 10^{-5} .$$

Assuming the same couplings for up and down quarks (i.e. $g^1=0$), the upper bound of the coupling constant g^0 obtained is

$$|g^0| < 2.5 \times 10^{-7} .$$

We wish to thank P. Reeve and A. Otter for assistance in magnet assembly and measurements, L.P. Robertson for help in the early stages, the NRC physics workshop for the construction of the TPC, J. Cresswell and the TRIUMF electronics shop for designing and building the electronics for the trigger system and gating grids, L. Raffler and the Carleton University Science Technology Center and M. Salomon, C. Stevens and the TRIUMF detector shop for construction of trigger counters, R.J. McKee, D. Kessler, W. Dey, D. Sample, S. Daviel, A. Bennett, C. Irwin and W.R. Jack for software development, and J. Legault, J. Stapledon, R. Bula and C. Lim for their technical help. This work was supported by the Natural Science and Engineering Research Council and the National Research Council of Canada.

References

- ¹G. Altarelli et al., Nucl. Phys. B125, 285 (1977).
²T.P. Cheng and L.F. Li, Phys. Rev. D16, 1425 (1977).
³J.D. Bjorken and S. Weinberg, Phys. Rev. Lett. 38, 622 (1977).
⁴W.J. Marciano and A.I. Sanda, Phys. Rev. Lett. 38, 1512 (1977).
⁵O. Shanker, Nucl. Phys. B206, 253 (1982).
⁶D.A. Bryman et al., Phys. Rev. Lett. 28, 1469 (1972).
⁷A. Badertscher et al., Nucl. Phys. A377, 406 (1982).
⁸C.K. Hargrove et al., Nucl. Instr. Meth. 219, 461 (1984).
⁹D.A. Bryman et al., Nucl. Instr. Meth. 234, 42 (1985).
¹⁰E.W. Blackmore et al., Nucl. Instr. Meth. 234, 235 (1985).
¹¹T. Suzuki, Ph.D thesis, University of British Columbia, 1980
 (unpublished).

Table I

TPC parameters		
Number of sectors	12	
Number of wires/sector	12	
Number of cathode pads/sector	636	
Wire spacing	2.54 cm	
Radial position of innermost wire	19.05 cm	
Wire diameter	20 μ m	
Drift length	34.3 cm	
Gas	Ar:CH ₄ (80:20) 1 atm	
Drift velocity	7 cm/ μ s	
Drift field	250 V/cm	
Gas gain	5x10 ⁴	

Table II

Correction factors for the total acceptance

$\pi^+\pi^-$ ev acceptance (includes following cuts)	Energy loss in TPC	0.12
Cosmic Ray	1.0	
Others	0.8	
χ^2 cut and visual inspection	0.9	
Pion background cut (beam)	0.9	
Target position cut	0.9	
Time window	0.7	
Energy window (97-105.5 MeV)	0.8	

Figure Captions

1. A cut-away view of the TPC. The numbered elements are: (1) the magnet iron, (2) the coil, (3a) and (3b) outer trigger scintillators, (4) outer trigger proportional counters, (5) end cap support frame, (6) inner electric field cage wires, (7) central high voltage plane, (8) outer electric field cage wires, (9) inner trigger scintillators, (10) inner trigger cylindrical proportional wire chamber, and (11) end cap proportional wire modules for track detection.
2. Solid histogram: experimentally observed events. Solid curve: Monte Carlo simulation for $\mu^- \rightarrow e^- \bar{\nu} \bar{\nu}$ decay in atomic orbit. Dashed histogram: Monte Carlo spectrum of $\mu^- Ti \rightarrow e^- Ti$ events for a branching ratio of 10^{-10} .

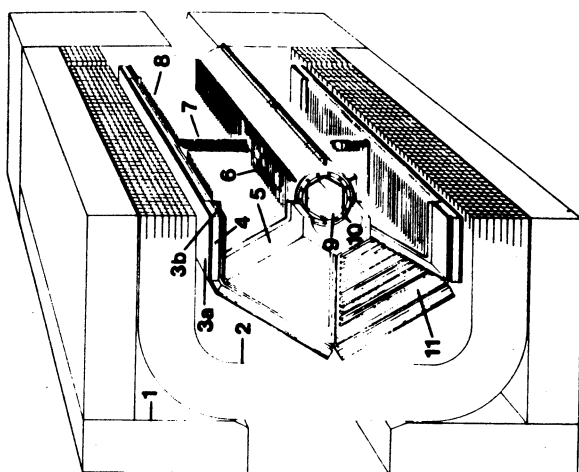


Fig. 1

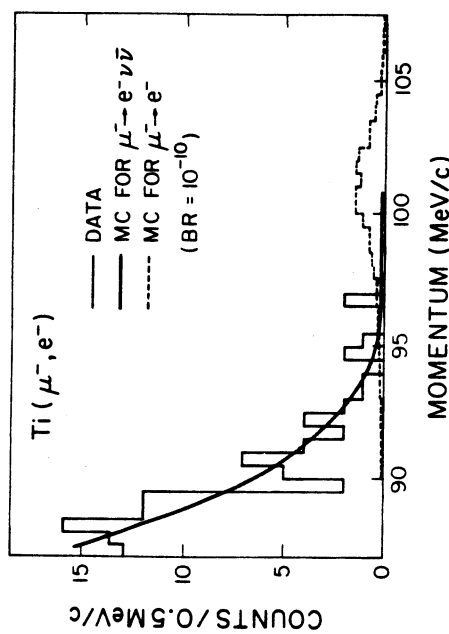


Fig. 2